High-resolution finite volume methods for extracorporeal shock wave therapy

Kirsten Fagnan[1], Randall J. LeVeque[1], Thomas J. Matula[2] and Brian MacConaghy[2]

[1] Department of Applied Mathematics, University of Washington, Box 352420, Seattle, WA, 98195 kfagnan@amath.washington.edu, rjl@amath.washington.edu

[2] Applied Physics Lab, University of Washington, Box 355640, Seattle, WA, 98195, matula@apl.washington.edu, brianm@apl.washington.edu

1 Introduction

Extracorporeal Shock Wave Therapy (ESWT) is a noninvasive technique for the treatment of a variety of musculoskeletal conditions such as delayed union of bone fractures, plantar fasciitis and calcified tendonitis of the shoulder. Shock waves were first used medically in the lithotripsy procedure (ESWL) to pulverize hardened calcified deposits such as kidney stones. This technique was then extended to musculoskeletal conditions as a treatment for calcifications in the shoulder, as these deposits are similar to renal calculi [1]. Later ESWT was shown to improve bone regeneration in the treatment of non-unions, which are bone fractures that fail to heal over time. In electrohydraulic lithotripsy, a shock wave is generated in a liquid bath, focused through the use of an ellipsoid reflector, and then propagates into the body where it ideally strikes the area of interest. Clinicians have indicated that this is not always the case and treatments will sometimes cause unforseen damage in parts of the body. Current numerical models are limited to simplified situations because the structure of the wave is highly nonlinear and therefore difficult to model with traditional finite difference and finite element techniques. We utilize high-resolution finite volume methods to capture the discontinuous pressure wave and model the wave propagation in bone and tissue. This approach has been successfully applied to many problems in acoustic or elastic wave propagation in heterogeneous media [2].

We are currently modeling shock wave propagation and reflection with linear elasticity equations, using finite volume methods in which each grid cell has material parameters associated to that cell. We use a Godunov-type method, which utilizes Riemann solvers in the wave propagation algorithm to solve the system of partial differential equations. Results were obtained in two- and three- dimensions using the CLAWPACK [3] and CHOMBOCLAW

[4] software packages. To provide validation of these results, our modeling effort is compared to experiments.

2 Background

2.1 Extracorporeal Shock Wave Therapy

The basic physics of the shock wave generation and propagation are well understood. A shock wave is a rapidly traveling pressure disturbance and is characterized by a sudden rise from ambient pressure to the maximum pressure in the system. As pressure increases, the velocity of the sound wave increases and therefore wave components at higher pressure move faster than those at lower pressure. Since the velocity of the wave components is dependent upon the pressure, the wave deforms and steepens into a shock.

Electrohydraulic lithotripters have a spark plug source that generates a spherical shock wave pulse in water, which can be modeled as an underwater explosion. The shock wave reflects off an ellipsoidal reflector, and propagates through the fluid into the body. Attenuation is limited through the use of a coupling gel between the membrane and skin. When the shock wave enters the body it will be reflected and dissipated depending upon the material parameters of the tissues that are in its path. Eventually the wave will collide with the intended target centered at the second focus of the ellipse, as is illustrated in Figure 1(b). An essential property of ESWL and ESWT is that, due to shock wave focusing, maximal energy should be deposited in the treatment area centered at the second focus of the ellipsoid.

A typical shock wave has a high peak pressure of approximately 50-80 MPa with a short life cycle of approximately 10 nanoseconds, followed by a negative pressure wave that lasts for a few microseconds[1]. The diagram in Figure 1(a) illustrates a typical wave form and its physical parameters as it would appear at the second focus. The tensile region is of particular interest, as it generates cavitation bubbles . This effect is one of the primary sources of energy leading to stone fragmentation in ESWL and is thought to contribute to the angiogenic response observed during ESWT treatments [5],[6]. Cavitation is not currently accounted for in our model. However, we have demonstrated with our results in section 3, that it is possible to numerically calculate regions of maximal tension, which correspond to areas of cavitation in the laboratory experiments.

2.2 Mathematical Model

There are generally two types of waves that can propagate in an elastic solid, namely P-waves (pressure or primary waves) and S-waves (shear or secondary waves). In one dimensional problems, these waves can be modeled by disjoint systems of equations. In higher dimensional problems, there is a coupling between P-waves and S-waves, so the situation is more complex. We aim to

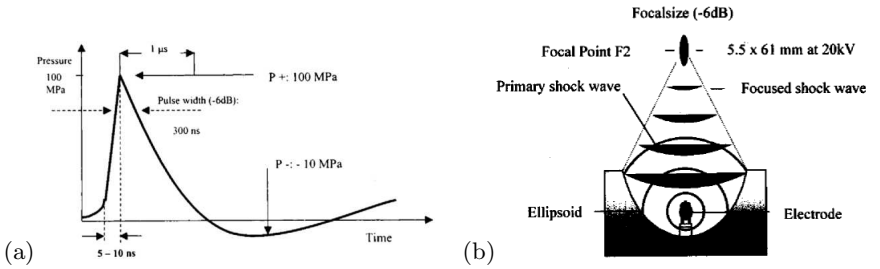

Fig. 1. Basic components of lithotripsy treatment. (a) The standard pressure wave profile at the second focus in lithotripsy and illustration of high pressure pulse followed by negative pressure or tensile region. (b) The basic setup for an electrohydraulic lithotripter. There is an ellipsoid reflector made of brass and a spark plug shock wave source at the F1 focus. [1]

model the behavior of these waves when propagating through soft tissue and bone in the body.

For the preliminary results presented here, we have used the 3D linear elasticity equations. We assume the soft tissue and bone are each isotropic materials and hence the equations have the form

$$\begin{aligned}
\sigma_t^{11} - (\lambda + 2\mu)u_x - \lambda v_y - \lambda w_z &= 0 \\
\sigma_t^{22} - \lambda u_x - (\lambda + 2\mu)v_y - \lambda w_z &= 0 \\
\sigma_t^{33} - \lambda u_x - \lambda v_y - (\lambda + 2\mu)w_z &= 0 \\
\sigma_t^{12} - \mu(v_x + u_y) &= 0 \\
\sigma_t^{23} - \mu(v_z + w_y) &= 0 \\
\sigma_t^{31} - \mu(u_z + w_x) &= 0 \\
\rho u_t - \sigma_x^{11} - \sigma_y^{12} - \sigma_z^{13} &= 0 \\
\rho v_t - \sigma_x^{12} - \sigma_y^{22} - \sigma_z^{23} &= 0 \\
\rho w_t - \sigma_x^{13} - \sigma_y^{23} - \sigma_z^{33} &= 0.
\end{aligned}$$

Here σ^{ij} represents the components of the stress tensor, $u = [u, v, w]$ are the components of velocity and λ and μ are the Lame parameters. We use this nonconservative form of the elasticiy equations to determine an analytical solution to the Riemann problem, which is the basis for the Reconstruct Evolve Average (REA) algorithm used in CLAWPACK [3].

The numerical tests presented here are compared to laboratory experiments where acrylic or acrylonitrile butadiene styrene (ABS) objects are immersed in water. We use the following values for the parameters:

$$\begin{aligned}
&\text{water}: \quad \rho = 1000 \ \ kg/m^3, \quad \lambda = 2190.4 \ \ MPa, \quad \mu = 0, \\
&\text{acrylic}: \rho = 1850 \ \ kg/m^3, \quad \lambda = 9305 \ \ MPa, \quad \mu = 3126.5 \ \ MPa, \\
&\text{ABS}: \quad \rho = 1210 \ \ kg/m^3, \quad \lambda = 3264 \ \ MPa, \quad \mu = 1032 \ \ MPa.
\end{aligned}$$

Each grid cell is assigned values of ρ, λ, and μ depending on which material it is in, or to averaged values of these parameters if an interface cuts through the cell.

This isotropic linear model is only a starting point. Modeling the shock wave formation and propagation more accurately requires using a nonlinear formulation of the elasticity equations, and ideally one would also incorporate anisotropic effects for soft tissue and bone. We are currently working on extending the model, but even this linear model gives results that capture some of the main features of experiments, as illustrated in the next section.

3 Results

We have been able to make comparisons between two- and three- dimensional laboratory and numerical experiments through an interdisciplinary collaboration at the University of Washington. Some of these results will be summarized here. Our collaborators at The Applied Physics Lab (APL) at the University of Washington, have performed several experiments with device similar to an HM3 Dornier lithotripsy device that we have used to verify our our numerical model [7]. In our numerical experiments we have solved the linear elasticity equations using high-resolution finite volume methods with adaptive mesh refinement.

3.1 Stress Wave Experiment

Figure 2 shows the results of an experiment where the stress waves in an acrylic cylinder are imaged using a high-speed camera and polarized filters. Acrylic is used because it is birefringent, allowing us to observe interior stress waves using polarizing optics[8]. The focus for the treatment is at the right edge of the cylinder and the shock wave propagates from right to left. There is a reflected wave resulting from interaction with the left edge of the cylinder. The photos show a conical shaped region where the stress is maximal. The location of the conical region agrees roughly with the fracture location of materials similar to kidney stones.

Figure 3 shows the numerical result of a pressure wave propagating through water and into an acrylic cylinder. We solve an axisymmetric version of the elasticity equations to generate these results. When we compare the numerical with the laboratory results in Figure 2, it is clear that our model has captured both the conical region of maximal stress and the reflection of the wave off the left edge of the cylinder. This indicates that the pressure wave in the solid is behaving like a linear elastic wave.

3.2 Cavitation Field Experiments

The primary objective of these experiments was to investigate the behavior of the shock wave as it interacts with a 3D representation of a talus bone.

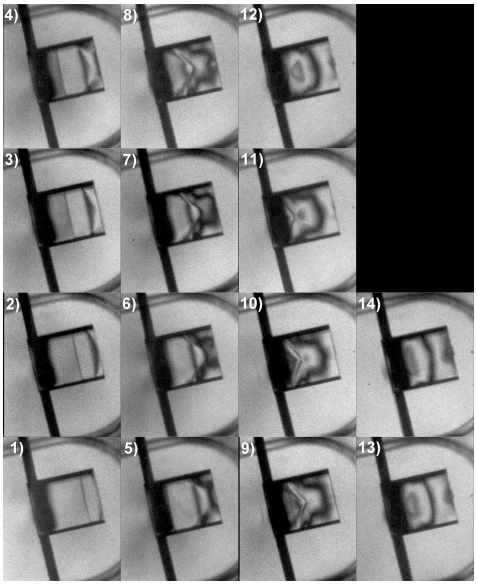

Fig. 2. Laboratory experiment where a shock wave is generated and propagates from right to left through an acrylic cylinder. The images are numbered to show the sequence in time. The stress waves are visualized using polarized film and images were taken with a high-speed camera. (courtesy of B. MacConaghy)

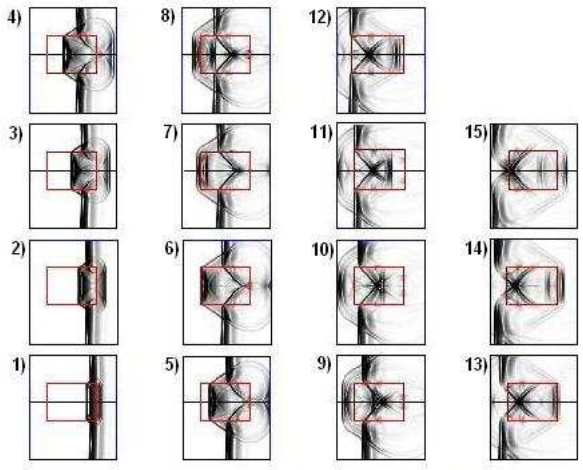

Fig. 3. A sequence of images from a numerical experiment for comparison with the laboratory result from Figure 2. The pressure wave propagates through the acrylic cylinder and the conical shaped, high-stress region develops in the simulation at a similar time and location to that of the lab experiment.

The bone is composed of ABS and was created by a group in the Mechanical Engineering Department at the University of Washington [9]. The three-dimensional digital representation of the bone that is used in the numerical experiments (see Figure 4), was provided by the same group. Therefore, we can make direct comparisons of our numerical results with the laboratory experiments.

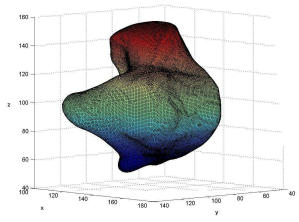

Fig. 4. A digital 3D representation of the talus used in the laboratory and numerical experiments [9].

The series of images in Figure 5 shows the deflection of the trail of cavitation bubbles or tensile component of the shock wave, as a function of bone placement within the field. As the location of the bone changes with respect to the focus, the deflection angle of the cavitation field is altered by the geometry of the bone. In some cases the cavitation field continues far past the desired treatment area and this could potentially cause tissue damage outside the focal region. The numerical results in Figure 6 show the maximum tensile component of the pressure wave along $y = 0$, a two-dimensional slice of the full 3D calculation. Each image shows the deflection of the shock wave's tensile component with different bone locations. The dot is the location of F2 and the bone is shifted in the z-direction relative to the focus as in Figure 5. The regions of maximum tension indicate where cavitation would occur, thus, this is the basis for comparison.

Due to the linear nature of the equations and computational limitations on the level of refinement, the pressure wave is more smeared out than in the laboratory experiment. As a result, the pressure wave interacts more with the front of the bone than the more focused laboratory shock wave. The deflection of the wave path due to the bone geometry is different from the laboratory result, however, the general behavior is similar in that there is an upward deflection of the cavitation path.

4 Conclusion

ESWT is a treatment for musculoskeletal conditions with its foundation in lithotripsy. Though clinical trials have indicated that this treatment is suc-

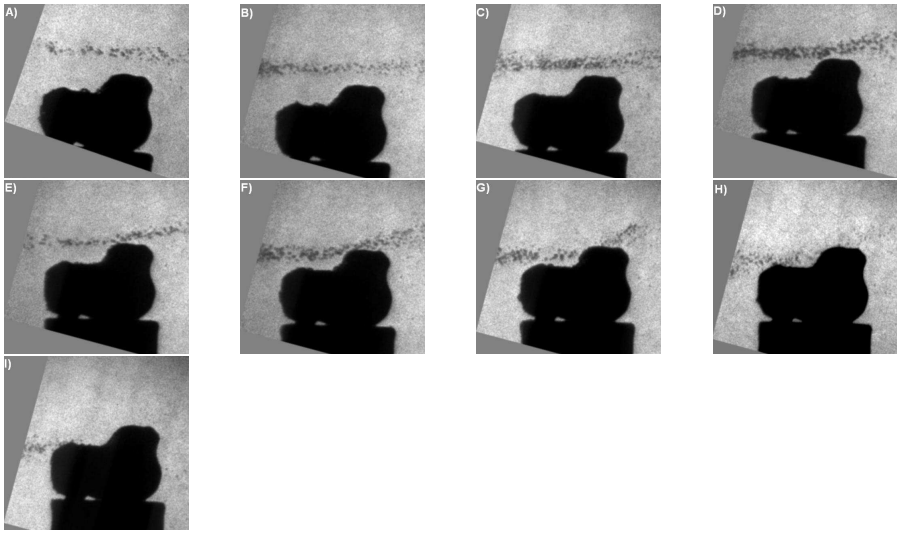

Fig. 5. Laboratory experiment where a shock wave is generated in the far left and the tensile component of the wave creates a cavitation field. The interaction of the cavitation field is imaged with a high-speed camera. The bone height changes from left to right where height corresponds to difference from the focus (A. -12, B. -9, C. -6, D. -3, E. 0, F. 3, G. 6, H. 9, I. 12)(courtesy of T. Matula).

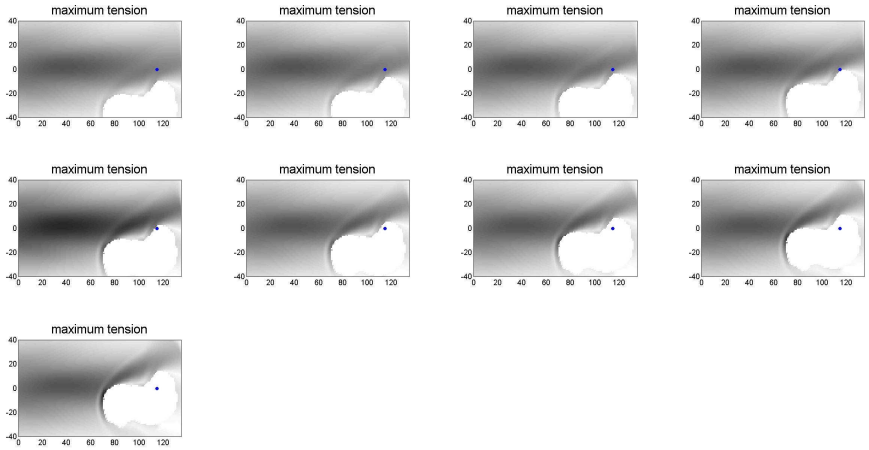

Fig. 6. Numerical simulation of laboratory experiment in Figure 5. These results demonstrate a dependence of the deflection angle on the placement of the bone with respect to F2. The blue dot is F2 and in each photo the bone placement is changing in z with respect to F2 (A. -12, B. -9, C. -6, D. -3, E. 0, F. 3, G. 6, H. 9, I. 12). Although the pressure wave is more smeared out than in the experiment, so there is more interaction with the front of the bone than in the laboratory experiment, the general behavior is correct.

cessful for a variety of conditions, the biological mechanisms are not well understood. We hope to model the propagation of the shock wave in bone and tissue so as to better understand this treatment. Our future goals include investigation on where energy is being deposited in the body and whether or not reflections from complicated geometry result in refocusing of the pressure wave.

We have used high-resolution finite volume methods and adaptive mesh refinement routines implemented in the CLAWPACK and CHOMBOCLOAW software packages, to solve the equations of linear elasticity in the isotropic materials. Results have been compared to two laboratory experiments where it is crucial to properly capture wave reflection at interfaces. Our preliminary results show reasonable qualitative agreement. In future work we plan to make more quantitative comparisons and to extend the model with the inclusion of nonlinear and non-isotropic effects to more accurately capture the ESWT pressure wave and the complex nature of bone and tissue.

5 Acknowledgments

This work was supported in part by DOE grant DE-FC02-01ER25474, NSF grant DMS-0106511, NIH grant PO1-DK043881, and an ARCS Foundation Founders Fellowship.

References

1. Anna Toth-Kischkat John A. Ogden and Reiner Schultheiss. Principles of shock wave therapy. *Clinical Orthopaedics and Related Research*, 387:8–17, 2001.
2. R.J. LeVeque. High-resolution finite-volume methods for acoustic waves in periodic and random media. *J. Acoust. Soc. Am.*, 106:17–28, July, 1999.
3. R.J. LeVeque. Clawpack software. http://www.amath.washington.edu/∼claw.
4. D. Calhoun. Chomboclaw software and documentation. http://www.amath.washington.edu/∼ calhoun/demos/chomboclaw/.
5. Robin O. Cleveland and Oleg A. Sapozhinikov. Modeling elastic wave propagation in kidney stones with application to shock wave lithotripsy. *Journal of the Acoustical Society of America*, 118(4):2667–2676, 2005.
6. H.Y. Huang C.J. Wang and C.H. Pai. Shock wave enhances neovascularization at the tendon-bone junction. *Journal of Foot and Ankle Surgery*, 41:16–22, 2002.
7. Robin O. Cleveland et al. Design and characterization of a research electrohydraulic lithotripter patterned after the dornier hm3. *Review of Scientific Instruments*, 71(6):2514–2525, 2000.
8. Xufeng Xi and Pe Zhong. Dynamic photoelastic study of the transient stress field in solids during shock wave lithotripsy. *Journal of the Acoustical Society of America*, 9(3):1226–1239, 2001.
9. D. Stuarti R.P. Ching, M. Ganter and Y. Hu. Mechanical engineering department. http://design.me.washington.edu/.